energies

MDPI

Article

Oxy-Fuel Combustion of Hard Coal, Wheat Straw, and Solid Recovered Fuel in a 200 kW_{th} Calcium Looping CFB Calciner

Joseba Moreno *, Matthias Hornberger, Max Schmid and Günter Scheffknecht

University of Stuttgart, Institute of Combustion and Power Plant Technology (IFK), Pfaffenwaldring 23, 70569 Stuttgart, Germany; matthias.hornberger@ifk.uni-stuttgart.de (M.H.); max.schmid@ifk.uni-stuttgart.de (M.S.); guenter.scheffknecht@ifk.uni-stuttgart.de (G.S.)
* Correspondence: joseba.moreno@ifk.uni-stuttgart.de

Abstract: The fluidized bed combustion (FBC) of biomass and solid recovered fuel (SRF) is globally emerging as a viable solution to achieve net-negative carbon emissions in the heat and power sector. Contrary to conventional fossil fuels, alternative fuels are highly heterogeneous, and usually contain increased amounts of alkaline metals and chlorine. Hence, experimental studies are mandatory in order to thoroughly characterize the combustion behavior and pollutant formation of non-conventional fuels in novel applications. This work gives an overview of experimental investigations on the oxy-fuel combustion of hard coal, wheat straw, and SRF with a limestone bed in a semi-industrial circulating fluidized bed (CFB) pilot plant. The CFB combustor was able to be operated under different fuel blending ratios and inlet O_2 concentrations, showing a stable hydrodynamic behavior over many hours of continuous operation. The boundary conditions introduced in this study are expected to prevail in carbon capture and storage (CCS) processes, such as the oxy-fuel combustion in the CFB calciner of a Calcium Looping (CaL) cycle for post-combustion CO_2 capture.

Keywords: oxy-fuel combustion; carbon capture; biomass combustion; SRF combustion; fluidized bed combustion; co-firing

Citation: Moreno, J.; Hornberger, M.; Schmid, M.; Scheffknecht, G. Oxy-Fuel Combustion of Hard Coal, Wheat Straw, and Solid Recovered Fuel in a 200 kW_{th} Calcium Looping CFB Calciner. *Energies* **2021**, *14*, 2162. https://doi.org/10.3390/en14082162

Academic Editor: Juliana Monteiro

Received: 26 February 2021
Accepted: 9 April 2021
Published: 13 April 2021

1. Introduction

Incineration is a well-established strategy for the valorization of refuse biomass and waste materials. The thermal utilization of alternative fuels allows the reduction of the volume of solids dumped in landfills, thereby decreasing greenhouse gas emissions and adverse health and environmental impacts. Processing residual waste to produce fuel is a common method applied to gain an increased value from refuse materials. The so-called solid recovered fuels (SRF) are standardized fuels produced from non-hazardous waste, intentionally prepared for quality criteria such as their calorific value, and mercury or chlorine content [1]. Today, biomass and biomass-based SRF are typically combusted in cement and power plants, either in stand-alone units or by co-firing them with fossil fuels [2,3]. Considering the challenges resulting from the intrinsic fuel characteristics (e.g., form and particle size, ash and moisture content), combustion systems need to be carefully designed in order to guarantee reliable plant operation and effective emissions control.

Circulating fluidized bed (CFB) systems are particularly well suited for the combustion of low-grade quality fuels due to their high fuel adaptability (i.e., low fuel processing efforts), increased solid residence time, and low pollutant emission. Moreover, CFB units might be applied within the framework of second-generation carbon capture and storage (CCS) processes. Carbon capture technologies collect the CO_2 emitted from the flue gases of power stations and industrial sites in order to provide a CO_2-rich stream suitable for capture after prior purification and compression. When applied to combustion processes, CCS technologies can be categorized into three groups: pre-combustion, post-combustion, and oxy-fuel. Besides this, the combination of biogenic fuels or fuels with a biogenic share (e.g., SRF) with carbon sequestration techniques enables net negative carbon emissions by

the sequestration of 'biogenic' CO_2. This approach is usually referred to as bioenergy with CCS (BECCS), which is gaining increasing popularity as a viable solution to counteract a potential overshoot of CO_2 emissions and meet the 2050 zero-carbon emission targets [4–8].

Over the past decades, Calcium Looping (CaL) has rapidly emerged as one of the most attractive second-generation CO_2 capture technologies. The CaL process uses natural limestone as a calcium oxide precursor (CaO) for CO_2 capture. The solid sorbent is continuously cycled between two interconnected fluidized bed reactors, utilizing the reversible carbonation reaction of CaO and the subsequent calcination of the formed $CaCO_3$ [9,10]. The CO_2 contained in the power plant's flue gas is exothermically absorbed by CaO in a carbonator at around 650 °C (see Figure 1). The CO_2-depleted flue gas is vented to the environment, whereas the partly-carbonated solids are transferred to a regeneration reactor (i.e., calciner). In the calciner, the CO_2 bound in the solid phase is released at around 900 °C. A gas stream highly concentrated in CO_2 leaves the regenerator, while the calcined sorbents are returned to the carbonator in order to close the solid loop. The heat required for the endothermic calcination reaction is provided by burning supplementary fuel with oxygen from an air separation unit (i.e., oxy-fuel combustion). The CO_2-rich regenerator flue gas can be partly recirculated into the system in order to maintain an appropriate combustion temperature. Due to sorbent deactivation upon cycling, a continuous flow of fresh make-up (i.e., $CaCO_3$) is fed to the process. This make-up flow is compensated by an equivalent sorbent purge in order to avoid the accumulation of inerts in the system (e.g., fuel ash and $CaSO_4$). So far, the CaL process has progressed steadily, being its feasibility demonstrated up to the MW_{th} scale using hard coal, lignite, and alternative fuels [11–15].

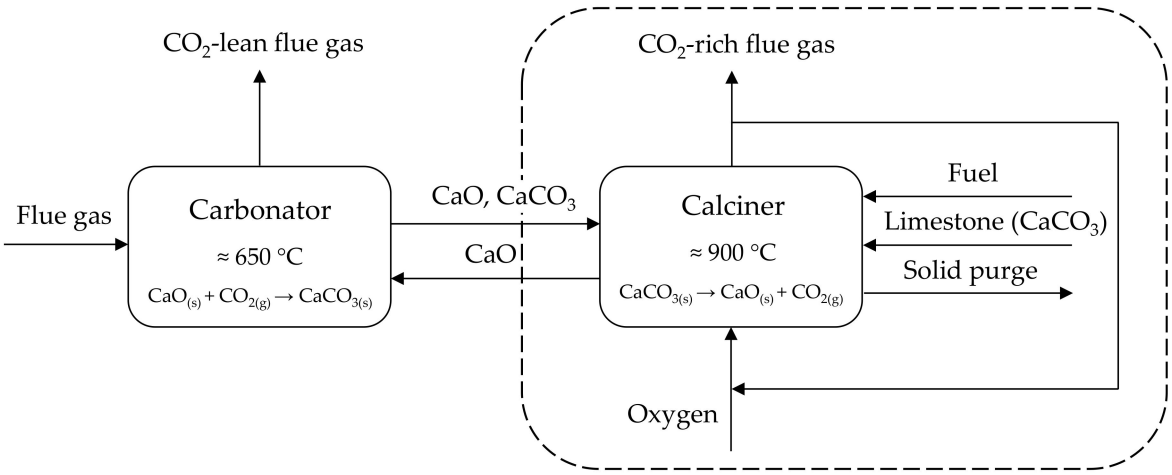

Figure 1. Schematic of the Calcium Looping process with the calciner enveloped in a dashed line.

Nitrogen oxides (NO_x) are critical components for the sequestration or utilization of CO_2, as they may cause corrosion due to the formation of nitric acid during the flue gas compression step [16]. In combustion systems, the main share of NO_x refers to NO, with the balance being NO_2 [17]. There are three routes which are responsible for NO_x formation (e.g., thermal, fuel, and prompt) [18]. Generally, CFB boilers are characterized by low NO_x emissions due to the moderate combustion temperatures, which prevent thermal NO_x formation [19,20]. Compared with CFB air combustion systems, the concentration of NO_x in the oxy-fuel case tends to be higher, whereas the specific NO_x conversion per fuel decreases [21]. This is derived from the significant reduction of the combustion flue gas due to the absence of airborne nitrogen. Compared with conventional oxy-fuel combustion, sorbent calcination in a Calcium Looping calciner might lead to enhanced NO_x emissions due to (i) the catalytic effect of CaO on NO_x formation and N_2O decomposition [22], (ii) the elevated temperature required for sorbent regeneration, and (iii) the increased oxygen concentration promoting the oxidation of nitrogen compounds and reducing the amount

of recirculated flue gas [21,23]. While NO_x formation during coal combustion in a CaL regenerator has been widely addressed in the past, much less attention has been devoted to NO_x emissions arising from a CaL calciner employing alternative fuels. To the best of the author's knowledge, there are no published studies which aimed to experimentally investigate the oxy-fuel mono-combustion of a non-woody biomass at a relevant CaL scale (TRL6). Moreover, at the time of writing, only one study has been reported on the investigation of NO_x formation under the stand-alone oxy-fuel combustion of SRF at a semi-industrial scale [24]. In the cited study, Haaf et al. aimed to compare two types of SRF, both under air-firing and oxy-fuel combustion conditions. The authors concluded that the specific NO emissions tend to be lower in the oxy-fuel case for both types of SRF and bed materials (i.e., sand and limestone), which was mainly attributed to the effect of flue gas recirculation during the oxy-fuel case.

Apart from CO_2 purity, utility boilers using alternative fuels might suffer severe problems such as slagging, fouling, and corrosion in heat exchangers. During combustion, alkali metals (M) and chloride are easily vaporized and released as alkali chlorides (MCl) into the flue gas. The gaseous alkali chlorides are then converted to alkali sulfates (M_2SO_4) through a homogeneous reaction with sulfur oxides and water vapor with or without oxygen (please refer to [25] for more details):

$$2\,MCl + SO_2 + H_2O + 1/2O_2 \rightarrow M_2SO_4 + 2\,HCl \quad (1)$$

$$2\,MCl + SO_3 + H_2O \rightarrow M_2SO_4 + 2\,HCl \quad (2)$$

The sulfation of such alkali chlorides releases chlorine as HCl, which is responsible for chlorine-induced high temperature corrosion [26]. In Calcium Looping applications, this problem is overcome to a great extent due to the capacity of limestone to absorb HCl at specific process conditions. The reaction of HCl with limestone in CFB systems is a complex, multi-layered process which mainly depends on the boiler temperature profile, prevailing gas atmosphere, and gas-solid contacting time [27–29]. To date, the absorption of HCl by Ca-species in fluidized beds has been mostly investigated at the laboratory scale [30,31], and only one pilot-scale study has been reported on the investigation of the fate of chlorine under oxy-fuel SRF combustion conditions [13].

The present work investigates the combustion characteristics of hard coal, wheat straw, and SRF under boundary conditions similar to those prevailing in an oxy-fuel CFB calciner of a Calcium Looping cycle. The study focuses on the implications of the fuel (blending) and inlet oxygen concentration on the emissions of NO_x and acidic gases (i.e., SO_2 and HCl), as well as on the process hydrodynamics. While NO_x emissions are discussed on the basis of the CO_2 purity criteria expected in compression and purification units (CPU), the focus with acidic gases is set on the ability of Calcium Looping solids to retain HCl. Throughout the introduced experiments, the CFB pilot plant demonstrated a high degree of fuel adaptability, allowing for many hours of continuous operation with stable hydrodynamic behavior. The experimental studies were carried out at the 200 kW_{th} CFB pilot plant of the University of Stuttgart, with industrially-relevant process conditions (i.e., recirculated flue gas and technically-pure oxygen).

2. Experimental Section

The University of Stuttgart's 200 kW_{th} CaL pilot facility consists of three refractory-lined fluidized bed reactors connected by a solid flow transport system [15,23]. For the experiments involved in this work, the CFB oxy-fuel combustor was used. A schematic of the installation is depicted in Figure 2.

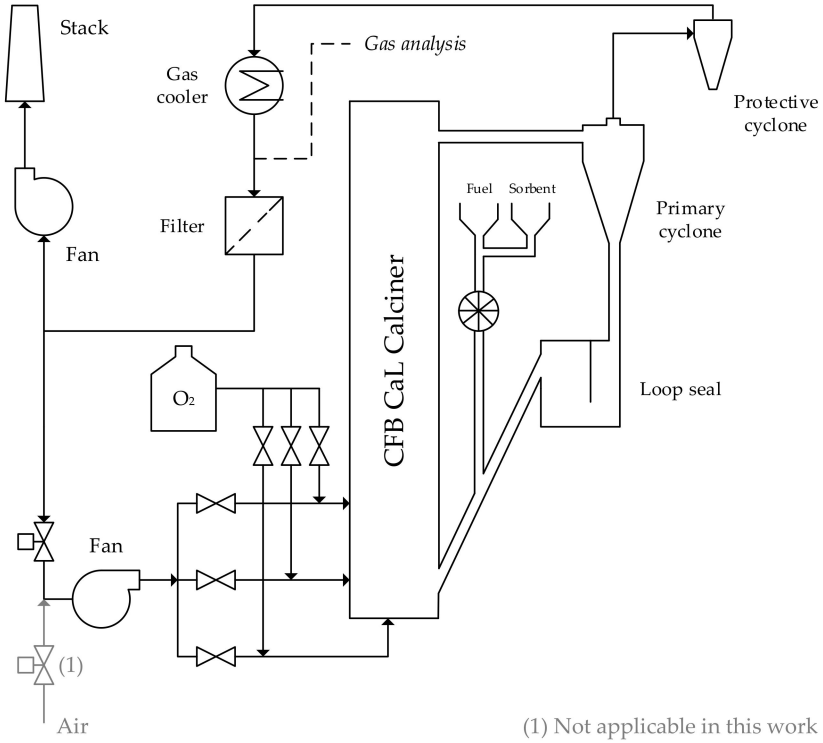

Figure 2. Schematic of the 200 kW_{th} Calcium Looping calciner.

The fully refractory lined CFB reactor has an average inner diameter of 200 millimeters and a total height of 10 meters. Sorbent particles are separated from the combustion flue gas in a primary cyclone, and are recirculated back to the reactor riser via a loop seal. The flue gas is then passed through a protective cyclone in order to ensure efficient solid separation before the gas cooler. After cooling the exhaust gas to approximately 180 °C, the gas undergoes particle clean-up in a baghouse filter before it is released to the environment or partly recirculated to the riser inlet. The combustion gas might consist of air, oxygen-enriched air, or recirculated flue gas and technically-pure oxygen. The gas mixture can be fed in three stages for the efficient control of the combustion temperature and pollutant formation. Solids (i.e., fuel and sorbent) are fed into the CFB unit using gravimetrically-controlled screw feeders. Bottom ash might be discharged by a bottom drain valve. Solid samples can be collected from the circulating solids in the loop seal, fly ash, and bottom ash. The flue gas composition is continuously measured by non-dispersive infrared spectroscopy (NDIR) (CO, CO_2, SO_2, NO_x), paramagnetism (O_2), and impact jet psychometry (H_2O) using online gas analyzers. Furthermore, other gas species of interest (e.g., HCl) can be measured by Fourier-transform infrared spectroscopy (FTIR). The volume fractions of CO_2, O_2, CO, SO_2 and NO_x are continously monitored using an ABB EL 3020, whereas continuous FTIR measurements are achieved using a portable system from Gasmet (DX4000). Gas sampling is conducted according to DIN EN 14792 [32] using a heated candle filter to separate particles from the sample gas, as well as a heated polytetrafluoroethylene (PTFE) hose and a heated pump in order to avoid condensation before the gas measuring unit. The particle filters are periodically cleaned by flushing nitrogen counter-currently. Throughout an experimental campaign, both the NDIR and the paramagnetic O_2 sensors are calibrated on a daily basis, and are recalibrated during the day if necessary. Within the first phase of the process, a zero calibration step with pure nitrogen is conducted. Subsequently, the gas analyzers are calibrated through a two-point procedure using gas cylinders of suitable composition. The calibration of the FTIR system is performed externally, and on a yearly basis. The gas sampling frequency is generally 1 s for the ABB EL 3020 and 20 s for the Gasmet DX4000.

The chemical composition (γ_i) and net calorific value (H_u) of the three fuels utilized in this work are introduced in Table 1. These consist of hard coal with a low sulfur content ('La Loma' mine, Colombia), pelletized and non-treated wheat straw (Agrarhandel Müller GbR, Germany), and pelletized SRF produced by steam-treating municipal solid waste (MSW) (ECONWARD, Spain). Table 2 summarizes the chemical composition of the limestone (x_i) used in the tests. The limestone type 'Messinghausener Sand 0.1–0.3' was obtained from Lhoist Germany Rheinkalk GmbH.

Table 1. Chemical composition (γ_i) and net calorific value (H_u) of the utilized fuels (waf: water and ash free; wf: water free; ad: air dried).

	γ_C	γ_H	γ_O	γ_N	γ_S	γ_{Cl}	γ_{ash}	γ_{H_2O}	H_u
	kg/kg, waf						**kg/kg, wf**	**kg/kg, ad**	**MJ/kg, ad**
Colombian hard coal	0.776	0.052	0.145	0.016	0.011	0.000	0.091	0.019	27.5
German wheat straw	0.497	0.066	0.425	0.010	0.001	0.001	0.059	0.081	15.6
Spanish SRF	0.515	0.067	0.377	0.026	0.006	0.009	0.261	0.067	14.3

Table 2. Chemical composition (x_i) of the utilized sorbent (wf: water free).

	x_{CaO}	x_{MgO}	x_{SiO_2}	$x_{Al_2O_3}$	x_{CO_2}	x_{others}
	kg/kg, wf					
German limestone	0.551	0.007	0.004	0.001	0.435	0.002

3. Evaluation Methodology

The concentration of the individual species in the flue gas can be introduced in multiple ways. The two approaches used throughout this publication are briefly explained below:

- y_i in ppmv: the volume fractions of NO_x, SO_2 and HCl measured in the flue gas at standard temperature and pressure (STP) conditions are presented in parts-per-million. y_{NO_x} and y_{SO_2} are given in dry conditions, whereas y_{HCl} is introduced on a wet basis.
- e_i in mg/MJ_{th}: in combustion processes, the emission factor of a gas pollutant 'i' is commonly described as the mass of pollutant released per unit of fuel burned [33]:

$$e_i = \frac{\dot{M}_i}{\dot{Q}_{th,H_u}} = \frac{\dot{V}_{FG,STP} \cdot y_i \cdot \rho_{n,i}}{H_u \cdot \dot{M}_B} \quad (3)$$

where the mass flow ($\dot{M}_i$) is calculated as the product of the flue gas volume flow in STP conditions ($\dot{V}_{FG,STP}$), and the volume fraction (y_i) and standard density ($\rho_{n,i}$) of the desired gas pollutant. The flue gas volume flow is continuously measured using an impeller anemometer, and is accordingly converted to STP conditions. Moreover, $\dot{Q}_{th,H_u}$ represents the thermal duty of a CFB combustor based on the mass flow ($\dot{M}_B$) and net calorific value (H_u) of the fuel.

Besides this, it is well known that limestone can absorb HCl under the operation conditions characteristic for fluidized bed boilers. Knowing the outlet volume fraction of HCl in the calciner flue gas, the chlorine retention rate (η_{HCl}) can be calculated according to Equation (4):

$$\eta_{HCl} = 1 - \frac{\dot{N}_{HCl,FG}}{\dot{N}_{Cl,B}} = 1 - \frac{(\dot{V}_{FG,STP} \cdot y_{HCl,FG} / V_{mn,HCl})}{(\dot{M}_B \cdot \gamma_{Cl,B} / \widetilde{M}_{Cl})} \quad (4)$$

where $\dot{N}_{HCl,FG}$ indicates the molar flow of HCl in the calciner flue gas, defined as the quotient between the product of the flue gas volume flow in STP conditions ($\dot{V}_{FG,STP}$) and the volume fraction of HCl in the exhaust gas ($y_{HCl,FG}$), and the standard molar volume of

HCl ($V_{mn,HCl}$). Furthermore, $\dot{N}_{Cl,B}$ represents the molar flow of chlorine entering the CFB unit, calculated according to the fuel mass flow ($\dot{M}_B$), the mass fraction of chlorine in the fuel ($\gamma_{Cl,B}$), and the molar mass of chlorine ($\widetilde{M}_{Cl}$).

4. Results

This study focused on the experimental evaluation of the oxy-fuel combustion characteristics of hard coal, wheat straw, and SRF under boundary conditions similar to those anticipated for the oxy-fuel CFB calciner of a Calcium Looping cycle. The results presented in this work are related to the CFB combustor's performance under different hard coal and biomass blending ratios and inlet oxygen concentrations in the oxidant gas. Additionally, the feasibility of the process under stand-alone SRF combustion is demonstrated. The evaluation of the CaL process concerning the CO_2 capture efficiency is out of the scope of this work.

4.1. Combustion of Hard Coal and Wheat Straw

Within the first phase of this study, a series of combustion tests were carried out by firing Columbian hard coal and non-woody German biomass (i.e., wheat straw). The effects of the combustion atmosphere and fuel blending ratio were systematically studied, maintaining the overall excess oxygen coefficient roughly constant throughout the tests. The different fuel blending ratios were defined according to the net calorific value of the different fuels, and were subsequently investigated at a similar temperature and oxy-fuel level (i.e., 910 ± 10 °C and 25 vol% O_2). Additionally, the impact of the inlet oxygen concentration was assessed at a temperature of 910 ± 10 °C with 30% biomass blending. Each experiment was conducted for at least 1 h (typically 2 h) under steady-state operating conditions. Moreover, the experiment with the mono-combustion of biomass was conducted for about 9 h, in order to assess the process performance on a longer-term basis.

4.1.1. Nitrogen Oxides (NO_x)

Figure 3a introduces the specific emission of nitrogen oxides (e_{NO_x}) measured during the investigation of four different hard coal and wheat straw combustion experiments. The depicted values refer to the average gas measurements obtained with NDIR and FTIR sensors, both placed at the same location (i.e., the sampling port) of the exhaust gas duct. The error bars represent the standard deviation of the measured value range.

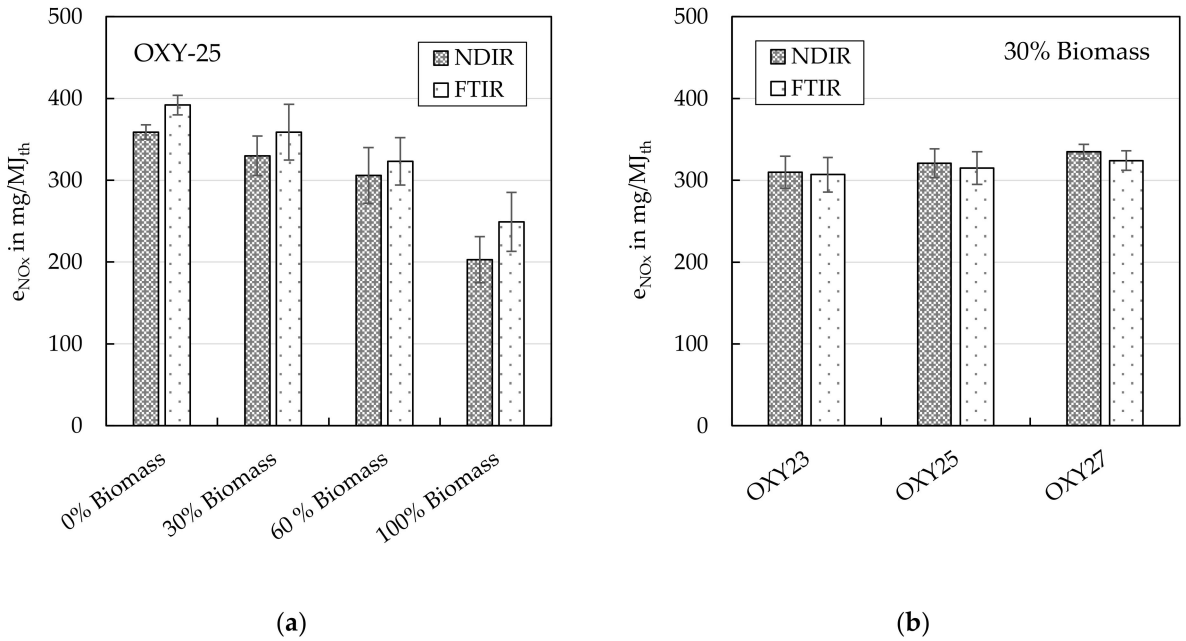

Figure 3. Specific NO_x emissions (e_{NO_x}) as a function of the biomass share ratio (**a**) and the oxy-fuel case (**b**).

According to the NDIR results, the specific NO_x levels ranged from 359 mg/MJ_{th} during combustion with 100% hard coal down to 203 mg/MJ_{th} with stand-alone biomass firing. As the fuel–NO_x formation mechanism is the dominating route under CFB conditions [34], this decrease can be ascribed to the reduced nitrogen content of the wheat straw (1.0 $wt\%_{waf}$) when compared to the fuel-N contained in the hard coal (1.6 $wt\%_{waf}$). This explanation is in line with the conclusions drawn by Riaza et al., who evaluated the NO emissions of blends of two distinct coal types with 10 wt% and 20 wt% olive waste under oxy-fuel conditions [35]. Riaza et al. concluded that the NO concentrations under an oxy-fuel atmosphere of both coals decreased after the addition of biomass, and reported an enhanced decrease as the biomass share was raised. Moreover, Figure 3b shows the specific NO_x emissions measured at different oxy-fuel levels under 30% biomass blending. From left to right, the depicted oxy-fuel cases correspond to inlet calciner dry oxygen concentrations of 23 vol%, 25 vol%, and 27 vol%, respectively. As no active cooling could be applied throughout the tests, the maximum attainable oxy-fuel case was limited by the target process temperature. Hence, an inlet oxygen concentration of 27 vol% was found to be the maximum in order to keep the desired reactor temperature of 910 °C. Moreover—as an attempt of maximizing the operating range—a minimum oxy-fuel case of 23 vol% was established. Furthermore, an oxy-fuel case of 25 vol% was evaluated for comparative purposes. The three different oxy-fuel cases in this study were established by adjusting the amount of recirculated flue gas. As the CFB calciner was operated under pure oxy-fuel combustion conditions, the air valve depicted in Figure 2 was kept closed during the tests. Within the investigated oxy-fuel range, the increased inlet oxygen concentrations led to slightly higher NO_x emissions (see Figure 3b). More precisely, an increase in the inlet oxygen volume fraction of about four percentage points caused a marginal increase in the specific NO_x NDIR emissions from 310 mg/MJ_{th} up to 335 mg/MJ_{th}. Providing a uniform temperature distribution along the reactor, the promoting effect of the inlet oxygen on NO_x emissions can be typically attributed to (i) the increased oxygen concentration intensifying the oxidation of the nitrogen components in the fuel [21,34], and (ii) the reduction in the flue gas recirculation rate causing the reducing zone of the calciner to be decreased [21]. However, within the relatively narrow investigated oxy-fuel range, it cannot be excluded that such deviations were, at least, partly attributable to fuel-N variations other than the aforementioned two reasons. In any case, the high NO_x emissions achieved in the CFB combustor operating at CaL calciner conditions will most certainly require an NO_x removal step before the CO_2 processing unit, depending on the required CO_2 specifications. Nevertheless, NO_x can be easily removed during compression in the CPU [16]. Elevated pressure favors the conversion from NO_x to NO_2, and NO_2 holds a high solubility, allowing it to form nitric acid by dissolving NO_2 in water after compression at around 30 bar in a dedicated contact column.

4.1.2. Acidic Gases (SO_2 and HCl)

The acidic gases emitted from combustion units may play a role in the corrosion of boiler components. In situ sulfur and halogen capture by limestone is one of the most important advantages of fluidized bed combustion (FBC). The use of a calcium-based sorbent (e.g., limestone) in fluidized bed boilers to reduce SO_2 emissions is a well-established technique. Limestone is introduced into the fluidized bed combustor at temperatures between 800 and 925°C, at which limestone is rapidly calcined to porous CaO, which can subsequently react with SO_2 to form calcium sulfite and calcium sulfate [36]. Furthermore, the addition of limestone can capture hydrogen chloride (HCl) to form liquid or solid phase calcium chloride under the relatively low combustion temperatures used in an FBC system [29]. The absorption of HCl by limestone can subsequently suppress the corrosion of heat exchanger tubes caused by chloride components, particularly when firing municipal solid waste or fuels with a high chlorine content. In Calcium Looping applications, both SO_2 and HCl are strongly suppressed due to (i) operation in a very favorable absorption temperature window [27,36] and (ii) an exceptionally high supply of calcium. The supply

of calcium which is available for SO_2 and HCl absorption is several magnitudes higher than that generally foreseen to remove SO_2 [25] and HCl [37] in fluidized bed combustion systems, yielding an almost sulfur- and chlorine-free flue gas.

Figure 4 depicts the specific emissions of SO_2 (e_{SO_2}) as a function of the biomass substitution ratio (graph a) and the oxy-fuel level applied (graph b). According to Figure 4a, there is a slight tendency in SO_2 emissions to decrease with increasing biomass substitution. Such a decreasing trend can be explained by (i) the significantly lower sulfur content of the wheat straw (0.001 $wt\%_{waf}$) compared with that of the hard coal (0.011 $wt\%_{waf}$), and (ii) the (partial) sulfation of alkali metal species contained in the fuel. Still, the decreasing tendency of e_{SO_2} in Figure 4a can be regarded as marginal. Because the thermal input to the reactor was maintained between the different tests, the stable behavior of e_{SO_2} can be ascribed to the mostly-constant SO_2 concentrations measured in the flue gas, which ranged between 1.9 mg/MJ_{th} and 2 mg/MJ_{th} (i.e., 3 ppmv) as a result of the very effective desulphurization rate achieved by the wide limestone availability (η_{SO_2} > 99 %). As far as the inlet oxygen concentration is concerned, it has been postulated that specific SO_2 emissions tend to be promoted in higher oxy-fuel cases [21,38]. However, the results obtained in this work (see Figure 4b) introduce a rather constant behavior of e_{SO_2} with increasing inlet O_2 as a result of the very effective in-situ flue gas desulphurization. With marginal differences between the investigated cases, e_{SO_2} averaged at 2 mg/MJ_{th}.

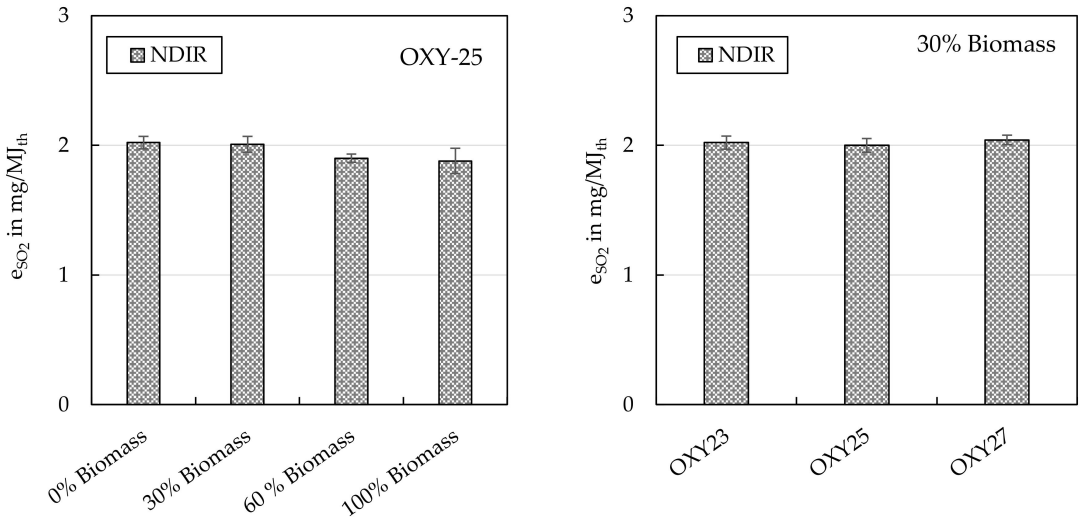

Figure 4. Specific SO_2 emissions (e_{SO_2}) as a function of the biomass share ratio (**a**) and the oxy-fuel case (**b**).

Figure 5 introduces the specific emissions of HCl (e_{HCl}) as a function of the biomass blending ratio (graph a) and the oxy-fuel level (graph b). According to Figure 5a, the specific HCl emissions increased from 1.8 mg/MJ_{th}, when no wheat straw was fired, up to 3.9 mg/MJ_{th}, with the mono-combustion of biomass. Here, as well, the explanation lies in the chlorine content of the fuels. Because the chlorine content in the biomass (0.1 $wt\%_{waf}$) is considerably higher than that in the hard coal (0.02 $wt\%_{waf}$), blending biomass increases the total chlorine content of the combusted fuel mix. These observations correlate well with the conclusions drawn by Wolf et al., who reported constantly-increasing HCl concentrations with growing shares of biomass when investigating the effect of the co-combustion of bituminous coal and straw in a CFB boiler [39]. Moreover, Figure 5b indicates a marginal increase in the specific HCl emissions during operation at higher inlet oxygen concentrations. However, as HCl is not an oxidation product, this behavior must be attributed to slight differences in the mass flow rates of hard coal and wheat straw between the tests.

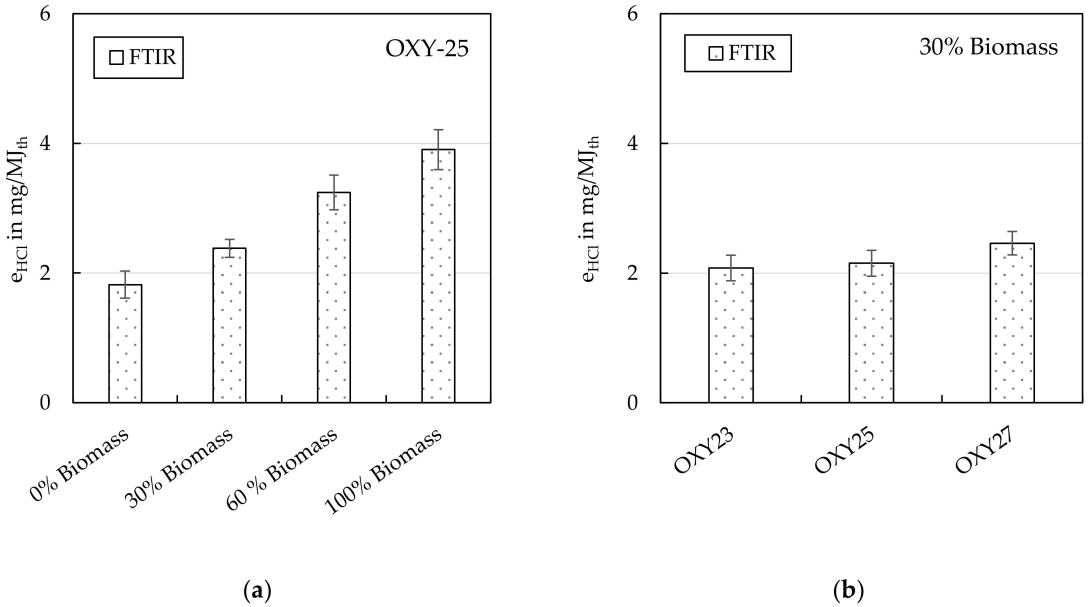

(**a**) (**b**)

Figure 5. Specific HCl emissions (e_{HCl}) as a function of the biomass share ratio (**a**) and the oxy-fuel case (**b**).

Besides this, the relatively low specific HCl emissions introduced in this study are greatly influenced by the capability of limestone to absorb HCl under specific Calcium Looping conditions. As anticipated previously, limestone can provide the efficient retention of SO_2 and HCl despite having different temperature regimes. Some authors have investigated the competitive mechanism between the sulfation and chlorination of calcined limestone, suggesting that the SO_2 retention efficiency is markedly promoted in the presence of HCl, while the concurrent chlorination reaction is suppressed [29,40]. As shown in Figures 4 and 5, both SO_2 and HCl emissions are strongly inhibited by the high calcium availability in the CFB calciner, which makes it difficult to provide a thorough assessment of the interaction between SO_2 and HCl in the system. Nonetheless, and recalling the capability of Calcium Looping solids to absorb hydrogen chloride, it is of practical interest to look into the chlorine retention rate achieved in each experiment (see Figure 6).

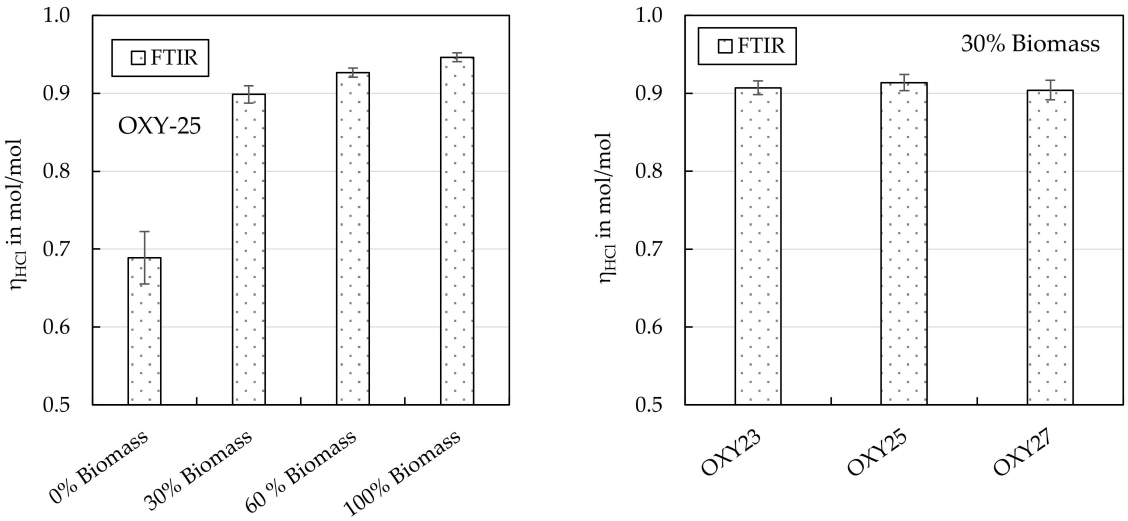

(**a**) (**b**)

Figure 6. HCl retention rate (η_{HCl}) as a function of the biomass share ratio (**a**) and the oxy-fuel case (**b**).

Figure 6a displays the average chlorine retention rate (η_{HCl}) calculated for all of the investigated fuel blending experiments. η_{HCl} averaged at 0.68 mol/mol during the stand-alone hard coal combustion, whereas 0.95 mol/mol was yielded during the mono-combustion of biomass. The comparatively high HCl retention efficiency achieved in the presence of biomass is presumably attributable to the increased content of alkali metal vapors, which can lead to more condensation nuclei during combustion and hence a higher absorption surface (i.e., limestone and/or ash) than pure hard coal combustion [41]. As can be observed in Figure 6a, chlorine retention rates above 0.90 mol/mol were obtained with at least 30% biomass substitution. The retention rate of HCl by limestone was also evaluated by Haaf et al. in a recent publication [13]. Haaf et al. investigated the mono-combustion of two SRF types at different temperatures in the calciner, and they reported retention values over 0.90 mol/mol for most of the conducted experiments. Moreover, the authors postulated that minimum calciner temperatures of around 860 °C are desirable to maximize chlorine retention (η_{HCl} > 0.90 mol/mol). Besides this, Figure 6b displays the marginal influence of the inlet oxygen concentration on the chlorine retention rate. Similarly to Figure 5b, this behavior can be attributed to slight differences in the respective coal and wheat straw flow rates, as HCl formation is not favored by the oxidizing atmosphere. Furthermore, it is true that HCl can react with O_2 under excessive oxygen atmospheres, releasing chlorine and water vapor according to the exothermic Deacon reaction [40]. Nevertheless, this latter effect was assumed to play a minor role in the present study, in which the high calciner temperatures will cause the equilibrium to move towards the reactants, which will lower the conversion of HCl to Cl_2. In view of the last results, it can be concluded that a Calcium Looping calciner can provide an appropriate framework for the reduction of HCl emissions originated by supplementary fuel combustion, lessening the associated impacts on equipment corrosion and the formation of polychlorinated dioxins and furans [42].

4.1.3. Reactor Profiles

Figure 7 shows the temperature (graphs a and c) and pressure (graphs b and d) profiles along the CFB riser for the different fuel blending and oxy-fuel cases investigated in this work. The riser height refers to the wind box nozzle top located at 0 m. Generally, the characteristics of the temperature profiles obtained for the different biomass share ratios correlate well with each other, showing average reference riser temperatures (i.e., 7.5 m) in the range of 914 to 918 °C (see Figure 7a). Besides this, while the temperature distributions obtained for 0%, 30%, and 60% biomass shares in the bottom section are comparable with each other, minor deviations were introduced at 100% biomass operation. The observed effect is attributed to the very distinct volatile matter of the hard coal (38.1 $wt\%_{wf}$) and the biomass (76.6 $wt\%_{wf}$). Like solid carbon, volatile components are not retained in the dense phase, which means that a major portion of the combustion reaction is taking place in the upper reactor zone. In consequence, wheat straw promotes high temperatures in the upper part and lower temperatures in the bottom section. Besides this, the temperature profiles observed during the investigation of the different oxy-fuel levels introduce the effect of increased oxygen addition (see Figure 7c). In order to evaluate this aspect, it is necessary to compare the gradual temperature increase observed between the lowest point where the oxidant is introduced (i.e., 0.25 m), and the height at which all of the oxidant has been added and adequately mixed (i.e., 5.5 m). After the subsequent comparison, temperature differences of 43 °C, 65 °C, and 68 °C were obtained for inlet oxygen concentrations of 23 vol%, 25 vol% and 27 vol%, respectively. As the fuel flow rate was kept constant between the tests, such temperature differences can be ascribed to an enhanced combustion thermal output arising from an increased inlet oxygen concentration. Despite the introduced deviations, the temperature profiles observed during the investigation of the diverse fuel blending and oxy-fuel experiments are smooth, and resemble a typical CFB combustor's uniform behavior without the presence of hot spots [23,43]. The influence of biomass co-firing on the CFB system's hydrodynamics can be observed in Figure 7b. The measured

pressure drop of the riser during biomass mono-combustion averaged at 40 mbar, which deviates considerably from the average value (i.e., 14 mbar) observed when no biomass was co-fired. For 100% biomass combustion, the pressure increases sharply in the dense zone, while above that, the decrease of the pressure blunts. Similarly to Figure 7a, this behavior can be ascribed to the higher amount of volatile matter contained in the biomass [44]. The increased volatile content of the wheat straw presumably causes a segregation in the solids along the reactor height, in which the reactor hydrodynamics range from the superposition of a bubble bed formed by coarser particles in the lower region, over a turbulent middle section with smaller particles, to a fast bed formed by fine particles in the upper part. Apart from this, it should not be ignored that the mono-combustion of biomass was investigated for 9 h of continuous operation. During this time, no material was drained from the system. Therefore, the described pressure increase can also be attributed, at least partially, to the effect of ash accumulation. Increased oxygen inlet concentrations did not have a significant influence on the pressure difference across the CFB riser (see Figure 7d). The pressure drop observed along the bed is very similar for all three investigated oxy-fuel cases, and indicates the absence of bed agglomeration effects.

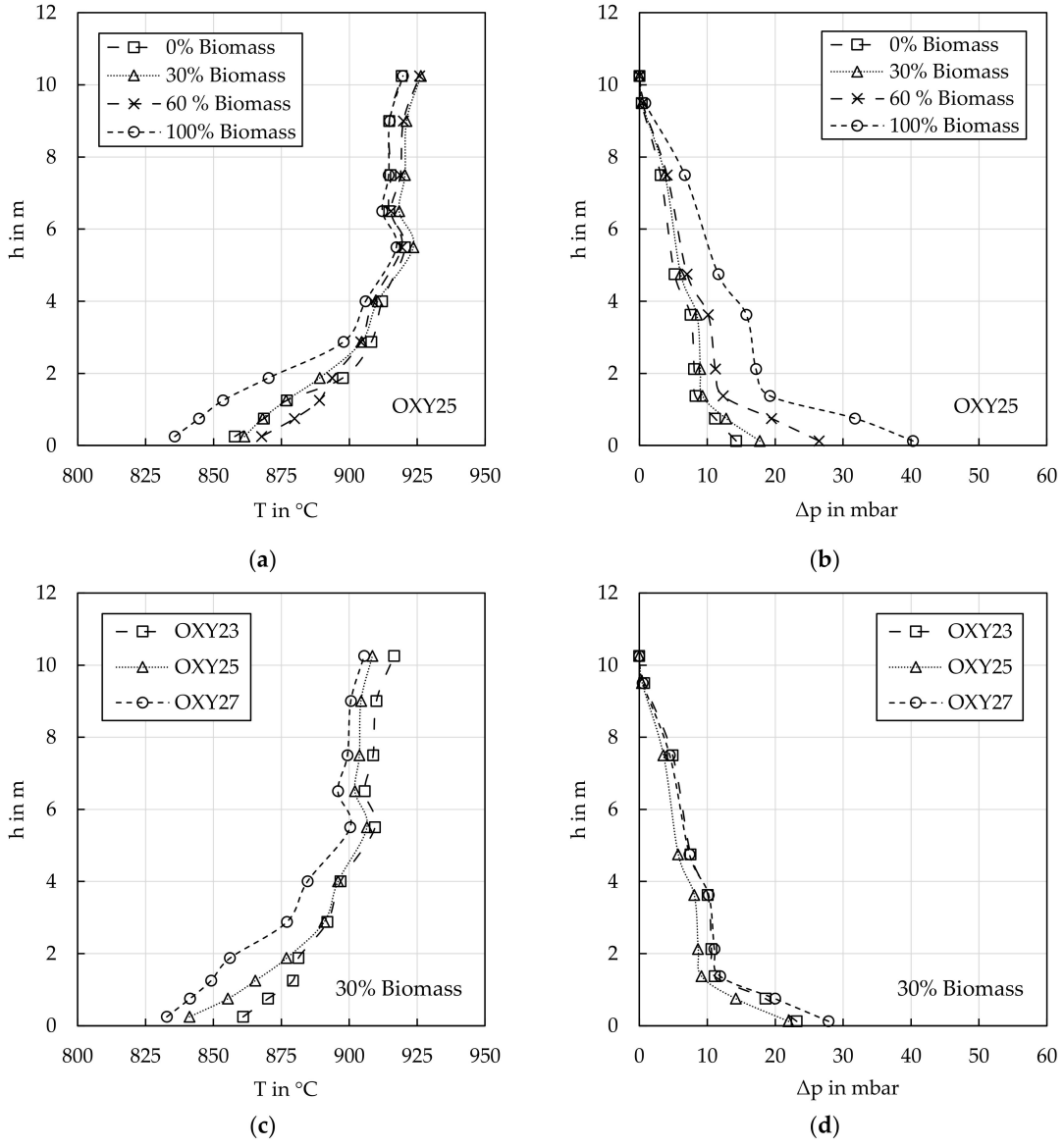

Figure 7. Calciner temperature (**a,c**) and pressure (**b,d**) profiles measured during the investigation of different fuel blending ratios and oxy-fuel cases.

4.2. Mono-Combustion of SRF

The overall goal of the following experiment was to demonstrate the feasibility of continuous and stable oxy-fuel SRF mono-combustion as a supplementary heat source in the CFB calciner. Table 3 provides an overview of the operating conditions throughout the experimental test. Generally, the selected conditions were similar to those defined for the investigation of the hard coal and biomass co-firing experiments, except for the combustion temperature. A technical limitation in the fuel dosing system constrained the maximum attainable temperature in the riser to approximately 865 °C. Accordingly, a reactor temperature of 850 °C was defined, aiming at exploiting the boundary conditions prevailing in municipal solid waste incinerators [45]. Of course, from the CaL sorbent calcination standpoint, temperatures above 900 °C are usually required to achieve efficient sorbent regeneration. In the 200 kW_{th} CFB calciner, this inconvenience can still be overcome due to the dilution of the CO_2 product stream in the reactor required for practical reasons, such as the flushing of pressure transducers, loop seal fluidization, and sealing purposes in the fuel feeding system. Hence, a sufficient sorbent calcination is feasible even at a calciner operation temperature in the range of 835 to 852 °C. The evolution of SRF stand-alone combustion is introduced in Figure 8. The left y-axis refers to the gas volume fractions of NO_x (y_{NO_x}), HCl (y_{HCl}), and SO_2 (y_{SO_2}), whereas the right y-axis shows the average riser temperature (T). The experimental time (t) is depicted in the x-axis.

Table 3. Experimental range of the operating conditions.

Parameter	Symbol	Value/Range	Unit
Temperature	T	835–852	°C
Thermal input	$\dot{Q}_{th}$	93–112	kW_{th}
Superficial gas velocity	u_0	3.9–4.1	m/s
Solid inventory	W_s	971–1479	kg/m^2
O_2 inlet volume fraction	$y_{O_2,in}$	0.21–0.22	m^3/m^3
Experimental duration	t	3.5	h

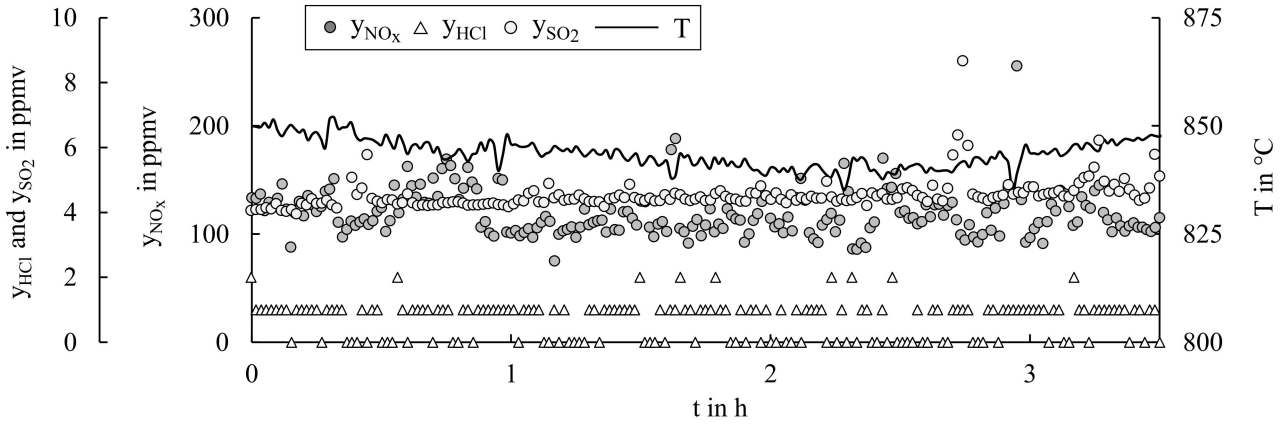

Figure 8. Volume fractions of NO_x (y_{NO_x}), HCl (y_{HCl}), SO_2 (y_{SO_2}), and temperature (T) against time (t) during solid recovered fuel mono-combustion. y_{NO_x} and y_{SO_2} were measured by non-dispersive infrared spectroscopy; y_{HCl} was measured by Fourier-transform infrared spectroscopy.

During the investigated period, the inlet oxygen concentration was close to 0.22 m^3/m^3. The oxygen excess at the calciner outlet was between 0.03 and 0.10 m^3/m^3, and averaged at 0.06 m^3/m^3 (on a dry basis). This relatively large oxygen excess was required in order to ensure the adequate burnout of the SRF. The thermal duty throughout the test averaged at 102 kW_{th}, and was similar to those investigated during the diverse co-firing experiments. The temperature fluctuations of the calciner were mainly caused by the inhomogeneous nature of the SRF. Moreover, several peaks can be observed roughly every 30 min, which

were ascribed to punctual irregularities in the fuel mass flow every time the dosing tank was re-filled. As can be observed, this effect did not have any significant influence on the stable and uniform evolution of the investigated gas species. HCl volume fractions up to 2 ppmv were measured downstream of the calciner, yielding an almost chlorine-free exhaust gas. The very low measured HCl concentrations in combination with the increased chlorine content of the SRF led to exceptionally high chlorine retention rates in the system, which yielded around 0.999 mol/mol. The SO_2 and NO_x concentrations showed a stable evolution throughout the test, and averaged at 4 ppmv and 127 ppmv, respectively. The minor fluctuations observed in Figure 8 are explained by side-effects caused by the re-filling of the fuel dosing unit (i.e., punctual changes in the excess oxygen level). Due to substantial differences in the combustion temperature, the NO_x concentrations displayed in Figure 8 cannot be directly referred to the trends obtained from the co-firing of hard coal and biomass. Nonetheless, the results introduced in this section are in line with the NO concentrations measured by Haaf et al. [13], considering the slight variations of the fuel composition and in the range of experimental conditions set for the respective tests.

Figure 9 shows the reactor temperature and pressure profiles measured during the mono-combustion of SRF. Similarly to Figure 7, the depicted temperature gradient is smooth, and resembles the operation of a typical CFB combustor (see Figure 9a). This is characterized by stable temperatures in the upper part and a gradual temperature increase in the bottom region. On the other hand, the solid induced pressure drop over the riser increased notably in the course of the experiment (see Figure 9b). More precisely, at the beginning of the test (t=0 h), the riser pressure drop was about 93 mbar, whereas this value averaged at 125 mbar after 3 h of continuous operation. Similarly to the mono-combustion of wheat straw, the depicted experiment was conducted without draining any solid bed material from the riser. Therefore, the increased bed pressure observed in this case can be attributed to ash accumulation effects. Moreover, the reactor pressure drops measured during the SRF mono-combustion were significantly higher than the differential riser pressures achieved during the investigation of the different biomass share ratios (see Figure 7b). This behavior can be explained by the different ash contents of the fuels. As introduced in Table 1, the ash content of the SRF (26.1 $wt\%_{wf}$) is considerably higher than the mass fraction of ash contained in the hard coal (9.1 $wt\%_{wf}$) and in the biomass (5.9 $wt\%_{wf}$). In any case, and in line with the observations made from the stand-alone biomass combustion, ash accumulation was found not to be a limiting aspect in this case either, and the CFB calciner was able to be fired with SRF under realistic oxy-fuel combustion conditions for several hours of continuous operation. Still, ash accumulation and agglomeration might constitute a major challenge for the stable and long term operation of industrial CFB boilers employing alternative fuels [46]. The common proposed measures to counteract ash-related issues include (i) operation at lower process temperatures, when possible; (ii) the dilution or renewal of the bed material; (iii) operation at increased fluidization velocities; and (iv) the incorporation of additives (e.g., kaolin). Furthermore, a reliable online monitoring system for the detection of early stages of ash-induced problems is crucial for the successful implementation of all of these measures [47]. However, the application of the proposed actions is not straightforward, as they need to be balanced by the criteria of CFB combustion efficiency and pollutant emission. In consequence, further investigation is still needed to cope with various challenges associated with ash accumulation effects.

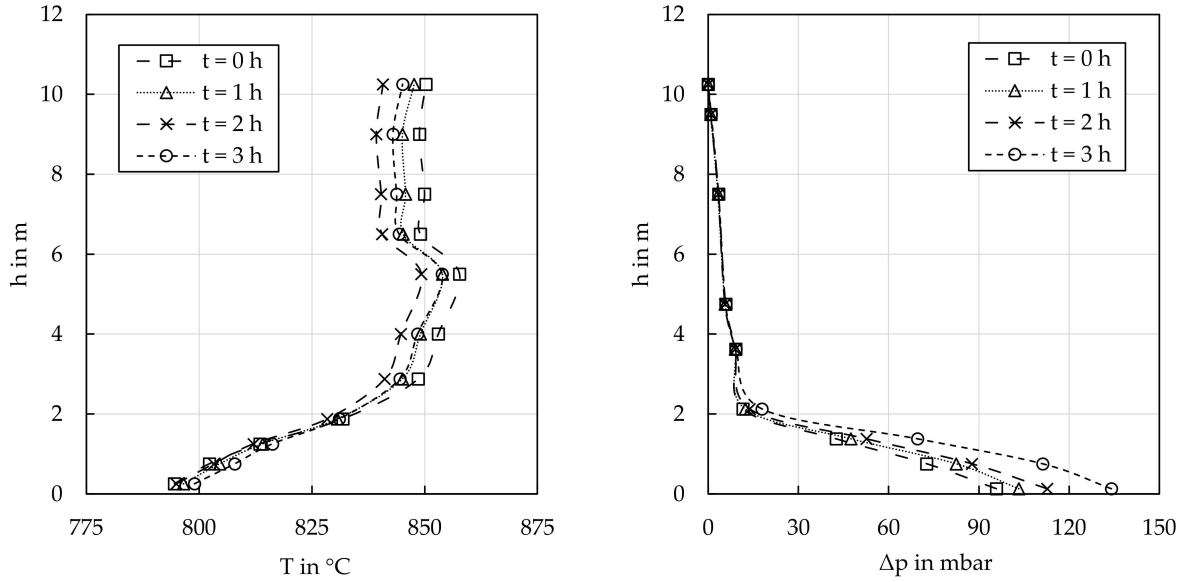

Figure 9. Calciner temperature (**a**) and pressure (**b**) profiles measured during solid recovered fuel mono-combustion.

5. Conclusions

In this work, the oxy-fuel combustion of hard coal, wheat straw, and solid recovered fuel was assessed at a semi-industrial 200 kW_{th} CFB test facility, under boundary conditions prevailing in the calciner of a CaL process. In the course of the pilot testing (of about 43 h), a wide range of experimental conditions were established. The fuel blending ratio and the inlet oxygen concentration were varied in order to derive implications about gaseous emissions of NO_x and acidic species such as SO_2 and HCl, as well as temperature and pressure reactor profiles. Fuel blending was found to hardly influence the pollution formation process. Nonetheless, biomass substitution directly affected the pollutant emissions by modifying the fuel mixture's nitrogen and chlorine content. HCl specific emissions were significantly reduced by the presence of Ca-species in the calciner, yielding chlorine retention rates above 0.90 mol/mol for all of the investigated experiments with biomass substitution. Moreover, the high NO_x emissions achieved in the CaL calciner will most certainly require a NO_x removal step before the CPU, depending on the required CO_2 specifications. The pilot reactor's temperature profile resembled the typical pattern described by conventional CFB units with no hot spots. Ash accumulation was found to significantly increase the pressure drop along the reactor not only at high biomass substitution rates but also during the mono-combustion of SRF. For the experiments in this study, the increased riser differential pressure was not a limiting aspect. Nevertheless, ash accumulation still constitutes a key challenge to be addressed in fluidized beds employing low-grade quality fuels in order to ensure reliable and long-term plant operation in novel CCS applications.

Author Contributions: Conceptualization, J.M.; methodology, J.M.; formal analysis, J.M.; investigation, J.M.; data curation, J.M.; writing—original draft preparation, J.M.; writing—review and editing, M.H., M.S. and G.S.; supervision, G.S. All authors have read and agreed to the published version of the manuscript.

Funding: This work was supported by the joint Research Fund for Coal and Steel (RFCS) research project 'FlexiCaL', under grant agreement No. 709629.

Acknowledgments: The authors gratefully acknowledge the financial support by RFCS, and would also like to thank the IFK's department 'Decentralized Energy Conversion' for its assistance during the diverse experimental campaigns.

Conflicts of Interest: The authors declare no conflict of interest.

Abbreviations

ad	air dried
B	fuel
BECCS	bio-energy with CCS
CaL	calcium looping
CCS	carbon capture and storage
CFB	circulating fluidized bed
CPU	compression and purification unit
FBC	fluidized bed combustion
FG	flue gas
FTIR	fourier-transform infrared spectroscopy
MSW	municipal solid waste
NDIR	non-dispersive infrared spectroscopy
PTFE	polytetrafluoroethylene
SRF	solid recovered fuel
STP	standard temperature and pressure
th	thermal
waf	water and ash free
wf	water free

Symbols

e_i	emission factor of gas component i (mg/MJ$_{th}$)
h	height (m)
H_u	net calorific value (MJ/kg)
$\dot{M}$	mass flow (kg/h or kg/s)
$\widetilde{M}_i$	molar mass of component i (kg/kmol)
$\dot{N}$	molar flow (kmol/h or kmol/s)
Δp	differential pressure (mbar)
$\dot{Q}$	heat flow (kW)
T	temperature (°C)
t	time, experimental duration (h)
u_0	superficial gas velocity (m/s)
$\dot{V}$	volume gas flow (m^3/h)
V_{mn}	standard molar volume (22.4 l/mol)
W_s	cross-sectional area based solid inventory (kg/m^2)
x_i	mass fraction of component i (kg/kg)
y_i	outlet gas volume fraction of component i (ppmv)
$y_{i,in}$	inlet gas volume fraction of component i (m^3/m^3)
η_i	retention rate of component i (mol/mol)
γ_i	fuel mass fraction of component i (kg/kg)
$\rho_{n,i}$	standard density of component i (kg/m^3)

References

1. RAL-GZ 724. *Sekundärbrennstoffe-Gütesicherung*; RAL Deutsches Institut für Gütesicherung und Kennzeichnung e. V.: Münster, Germany, 2012.
2. Sarc, R.; Lorber, K.E.; Pomberger, R. Manufacturing of Solid Recovered Fuels (SRF) for Energy Recovery Processes. *Waste Manag.* **2016**, *6*, 401–416.
3. Iacovidou, E.; Hahladakis, J.; Deans, I.; Velis, C.; Purnell, P. Technical properties of biomass and solid recovered fuel (SRF) co-fired with coal: Impact on multi-dimensional resource recovery value. *Waste Manag.* **2018**, *73*, 535–545. [CrossRef] [PubMed]
4. United Nations Treaty Collection. *The Paris Agreement*; Chapter XXVII 7 d; United Nations Framework Convention on Climate Change (UNFCCC): Paris, France, 2015.
5. Bui, M.; Fajardy, M.; Mac Dowell, N. Thermodynamic Evaluation of Carbon Negative Power Generation: Bio-energy CCS (BECCS). *Energy Procedia* **2017**, *114*, 6010–6020. [CrossRef]
6. Gough, C.; Upham, P. Biomass energy with carbon capture and storage (BECCS or Bio-CCS). *Greenh. Gases Sci. Technol.* **2011**, *1*, 324–334. [CrossRef]
7. Ditaranto, M.; Becidan, M.; Stuen, J. Opportunities for CO_2 Capture in the Waste-to-Energy Sector. *Waste Manag.* **2019**, *9*, 319–328.

8. Wienchol, P.; Szlęk, A.; Ditaranto, M. Waste-to-energy technology integrated with carbon capture—Challenges and opportunities. *Energy* **2020**, *198*, 117352. [CrossRef]
9. Shimizu, T.; Hirama, T.; Hosoda, H.; Kitano, K.; Inagaki, M.; Tejima, K. A Twin Fluid-Bed Reactor for Removal of CO_2 from Combustion Processes. *Chem. Eng. Res. Des.* **1999**, *77*, 62–68. [CrossRef]
10. Abanades, J.C.; Anthony, E.J.; Wang, J.; Oakey, J.E. Fluidized Bed Combustion Systems Integrating CO_2 Capture with CaO. *Environ. Sci. Technol.* **2005**, *39*, 2861–2866. [CrossRef] [PubMed]
11. Haaf, M.; Hilz, J.; Peters, J.; Unger, A.; Ströhle, J.; Epple, B. Operation of a 1 MW_{th} calcium looping pilot plant firing waste-derived fuels in the calciner. *Powder Technol.* **2020**, *372*, 267–274. [CrossRef]
12. Arias, B.; Diego, M.; Abanades, J.; Lorenzo, M.; Diaz, L.; Martínez, D.; Alvarez, J.; Sánchez-Biezma, A. Demonstration of steady state CO_2 capture in a 1.7MW_{th} calcium looping pilot. *Int. J. Greenh. Gas Control.* **2013**, *18*, 237–245. [CrossRef]
13. Haaf, M.; Peters, J.; Hilz, J.; Unger, A.; Ströhle, J.; Epple, B. Combustion of solid recovered fuels within the calcium looping process—Experimental demonstration at 1 MW_{th} scale. *Exp. Therm. Fluid Sci.* **2020**, *113*, 110023. [CrossRef]
14. Vorrias, I.; Atsonios, K.; Nikolopoulos, A.; Nikolopoulos, N.; Grammelis, P.; Kakaras, E. Calcium looping for CO_2 capture from a lignite fired power plant. *Fuel* **2013**, *113*, 826–836. [CrossRef]
15. Dieter, H.; Bidwe, A.R.; Varela-Duelli, G.; Charitos, A.; Hawthorne, C.; Scheffknecht, G. Development of the calcium looping CO_2 capture technology from lab to pilot scale at IFK, University of Stuttgart. *Fuel* **2014**, *127*, 23–37. [CrossRef]
16. Shah, M.; Degenstein, N.; Zanfir, M.; Kumar, R.; Bugayong, J.; Burgers, K. Near zero emissions oxy-combustion CO_2 purification technology. *Energy Procedia* **2011**, *4*, 988–995. [CrossRef]
17. Scheffknecht, G.; Al-Makhadmeh, L.; Schnell, U.; Maier, J. Oxy-fuel coal combustion—A review of the current state-of-the-art. *Int. J. Greenh. Gas Control.* **2011**, *5*, S16–S35. [CrossRef]
18. Stanger, R.; Wall, T.; Spörl, R.; Paneru, M.; Grathwohl, S.; Weidmann, M.; Scheffknecht, G.; McDonald, D.; Myöhänen, K.; Ritvanen, J.; et al. Oxyfuel combustion for CO_2 capture in power plants. *Int. J. Greenh. Gas Control.* **2015**, *40*, 55–125. [CrossRef]
19. Pang, L.; Shao, Y.; Zhong, W.; Gong, Z.; Liu, H. Experimental study of NO_x emissions in a 30 kW_{th} pressurized oxy-coal fluidized bed combustor. *Energy* **2020**, *194*, 116756. [CrossRef]
20. Krzywanski, J.; Czakiert, T.; Shimizu, T.; Majchrzak-Kuceba, I.; Shimazaki, Y.; Zylka, A.; Grabowska, K.; Sosnowski, M. NO_x Emissions from Regenerator of Calcium Looping Process. *Energy Fuels* **2018**, *32*, 6355–6362. [CrossRef]
21. Hofbauer, G. Experimentelle Untersuchung der Oxy-Fuel-Verbrennung von Steinkohle in einer zirkulierenden Wirbelschichtfeuerung. *Univ. Stuttg.* **2017**. [CrossRef]
22. Liu, H.; Gibbs, B. The influence of calcined limestone on NO_x and N_2O emissions from char combustion in fluidized bed combustors. *Fuel* **2001**, *80*, 1211–1215. [CrossRef]
23. Hornberger, M.; Moreno, J.; Schmid, M.; Scheffknecht, G. Experimental investigation of the calcination reactor in a tail-end calcium looping configuration for CO_2 capture from cement plants. *Fuel* **2021**, *284*, 118927. [CrossRef]
24. Haaf, M.; Müller, A.; Unger, A.; Ströhle, J.; Epple, B. Combustion of solid recovered fuels in a semi-industrial circulating fluid-ized bed pilot plant—Implications of bed material and combustion atmosphere on gaseous emissions. *VGB PowerTech.* **2020**, *3*, 51–56.
25. Lupiáñez, C.; Mayoral, M.C.; Díez, L.I.; Pueyo, E.; Espatolero, S.; Andrés, J.M. The role of limestone during fluidized bed oxy-combustion of coal and biomass. *Appl. Energy* **2016**, *184*, 670–680. [CrossRef]
26. Spliethoff, H. *Power Generation from Solid Fuels*; Springer: Berlin, Germany, 2010; ISBN 9783642028557.
27. Partanen, J.; Backman, P.; Backman, R.; Hupa, M. Absorption of HCl by limestone in hot flue gases. Part I: The effects of temperature, gas atmosphere and absorbent quality. *Fuel* **2005**, *84*, 1664–1673. [CrossRef]
28. Partanen, J.; Backman, P.; Backman, R.; Hupa, M. Absorption of HCl by limestone in hot flue gases. Part II: Importance of calcium hydroxychloride. *Fuel* **2005**, *84*, 1674–1684. [CrossRef]
29. Partanen, J.; Backman, P.; Backman, R.; Hupa, M. Absorption of HCl by limestone in hot flue gases. Part III: Simultaneous absorption with SO_2. *Fuel* **2005**, *84*, 1685–1694. [CrossRef]
30. Piao, G.; Aono, S.; Kondoh, M.; Yamazaki, R.; Mori, S. Combustion test of refuse derived fuel in a fluidized bed. *Waste Manag.* **2000**, *20*, 443–447. [CrossRef]
31. Desroches-Ducarne, E.; Marty, E.; Martin, G.; Delfosse, L.; Nordin, A. Effect of Operating Conditions on HCl Emissions from Municipal Solid Waste Combustion in a Laboratory-Scale Fluidized Bed Incinerator. *Environ. Eng. Sci.* **1998**, *15*, 279–289. [CrossRef]
32. DIN EN 14792. In *Stationary Source Emissions—Determination of Mass Concentration of Nitrogen Oxides—Standard Reference Method: Chemiluminescence*; DIN German Institute for Standardization: Berlin, Germany, 2017.
33. Trozzi, C. *EMEP/EEA Air Pollution Emission Inventory Guidebook 2019: Energy Industries*; European Environment Agency: Copenhagen, Denmark, 2019.
34. Pu, G.; Zan, H.; Du, J.; Zhang, X. Study on NO Emission in the Oxy-Fuel Combustion of Co-Firing Coal and Biomass in a Bub-bling Fluidized Bed Combustor. *BioResources* **2016**, *12*, 1890–1902. [CrossRef]
35. Riaza, J.; Gil, M.; Álvarez, L.; Pevida, C.; Pis, J.; Rubiera, F. Oxy-fuel combustion of coal and biomass blends. *Energy* **2012**, *41*, 429–435. [CrossRef]
36. De Diego, L.; Rufas, A.; García-Labiano, F.; Obras-Loscertales, M.D.L.; Abad, A.; Gayán, P.; Adánez, J. Optimum temperature for sulphur retention in fluidised beds working under oxy-fuel combustion conditions. *Fuel* **2013**, *114*, 106–113. [CrossRef]

37. Cai, Y.; Ma, Z.; Yan, J.; Zhang, Y.; Chen, Z.; Gao, R.; Zhong, P. Dichlorination in a circulating fluidized-bed incinerator for municipal solid waste incineration system. *Waste Dispos. Sustain. Energy* **2019**, *1*, 207–212. [CrossRef]
38. Hu, Y.; Naito, S.; Kobayashi, N.; Hasatani, M. CO_2, NO_x and SO_2 emissions from the combustion of coal with high oxygen concentration gases. *Fuel* **2000**, *79*, 1925–1932. [CrossRef]
39. Wolf, C.; Leino, T.J.; Stephan, A.R.; Aho, M.J.; Spliethoff, H. Online Corrosion Measurements in Combination with Deposit and Aerosol Analysis during the Co-firing of Straw with Coal in Electrically Heated, Small-Scale Pulverized Fuel and Circulating Fluidized Bed Systems. *Energy Fuels* **2018**, *32*, 2506–2516. [CrossRef]
40. Xie, W.; Liu, K.; Pan, W.-P.; Riley, J. Interaction between emissions of SO_2 and HCl in fluidized bed combustors. *Fuel* **1999**, *78*, 1425–1436. [CrossRef]
41. Hu, G.; Dam-Johansen, K.; Wedel, S.; Hansen, J.P. Enhancement of the Direct Sulfation of Limestone by Alkali Metal Salts, Calcium Chloride, and Hydrogen Chloride. *Ind. Eng. Chem. Res.* **2007**, *46*, 5295–5303. [CrossRef]
42. Addink, R.; Bakker, W.C.M.; Olie, K. Influence of HCl and Cl_2 on the Formation of Polychlorinated Diben-zo-p-dioxins/Dibenzofurans in a Carbon/Fly Ash Mixture. *Environ. Sci. Technol.* **1995**, *29*, 2055–2058. [CrossRef] [PubMed]
43. Dieter, H.; Hawthorne, C.; Zieba, M.; Scheffknecht, G. Progress in Calcium Looping Post Combustion CO_2 Capture: Successful Pilot Scale Demonstration. *Energy Procedia* **2013**, *37*, 48–56. [CrossRef]
44. Scala, F.; Salatino, P. Modelling fluidized bed combustion of high-volatile solid fuels. *Chem. Eng. Sci.* **2002**, *57*, 1175–1196. [CrossRef]
45. Dri, M.; Canfora, P.; Antonopoulos, I.S.; Gaudillat, P. Best Environmental Management Practice for the Waste Management Sector. *JRC Sci. Policy Rep.* **2018**. [CrossRef]
46. Bolhàr-Nordenkampf, M.; Nummelin, T.; Luomaharju, T.; Viljanen, J. Operating Experience from the World´s Largest Waste Fired Circulating Fluidized Bed Reactor in Västerås. *Waste Manag.* **2015**, *5*, 167–178.
47. Gatternig, B. *Predicting Agglomeration in Biomass Fired Fluidized Beds*; University of Erlangen-Nürnberg: Erlangen, Germany, 2015.